Available online at www.sciencedirect.com
SCIENCE DIRECT®
PERGAMON
International Journal of Impact Engineering 28 (2003) 377–390
INTERNATIONAL JOURNAL OF IMPACT ENGINEERING
www.elsevier.com/locate/ijimpeng

Plate perforation by eroding rod projectiles ☆

D.J. Gee*

Institute for Advanced Technology, The University of Texas at Austin, Austin, TX 78759, USA

Received 7 January 2002; received in revised form 8 August 2002

Abstract

The penetration and perforation of stationary, oblique steel plates by hypervelocity tungsten-alloy projectiles is examined here. Simulations have been performed for L/D 10 projectiles against one- and two-plate target configurations. The plate thickness-to-rod diameter ratio t/D varied slightly, as did the plate spacing-to-plate thickness ratio t_{gap}/t. For all simulations, $t/D \in [1.2, 1.6]$ and $t_{gap}/t \in [0.7, 1]$. Normalized line-of-sight perforation is one measure of performance, and archival test data are compared on this basis. The results presented reflect pre-impact aerodynamic pitch and yaw in the test data, but only pitch angle deviation in the numerical data. Simulation and test data are reasonably well correlated and the data suggest that a favorable pitch angle exists and may be related to impact geometry. By way of the numerical simulation, differences in perforation efficiency for one- and two-plate targets are noted and erosion mechanisms are explored. It is shown that projectile erosion between target plates depends, to an extent, upon plate spacing. Additionally, the data suggests that behind-plate residual erosion varies with the number of plates, decreasing as the number of plates increases.

Keywords: Perforation; Finite thickness plate; Erosion; Computational solid mechanics

1. Introduction

It is well known that tungsten projectiles seem to erode excessively while perforating thin steel plates. That is, by comparison the penetration of a semi-infinite thick target at comparable impact velocity is achieved with significantly higher penetration efficiency P/L (or depth of penetration normalized by projectile length) [1]. To gain insight into this phenomenon, a numerical study has been initiated on the perforation of stationary, finite thickness, oblique steel plates by slender

☆This paper is based in part on work presented at the 19th International Symposium on Ballistics, Interlaken, Switzerland, May 2001.

*Fax: +1-512-471-9096.
E-mail address: dgee@iat.utexas.edu (D.J. Gee).

0734-743X/02/$ - see front matter
PII: S0734-743X(02)00070-2

Nomenclature

A, B, C, m, n	Johnson–Cook constitutive model parameters
D, L	projectile diameter, length
$\dot{e}_{ij}^{p}$	deviatoric plastic strain-rate tensor
J_2	quadratic invariant for deviatoric stress tensor ($= 1/2 S_{ij} \cdot S_{ij}$)
t	plate thickness in direction of unit normal, time
t_{gap}	plate spacing
t_{los}	line-of-sight plate thickness
T, T_M, T_R	temperature, melt temperature, room temperature
u, v	penetration velocity, tail velocity
V_0, V_R	impact velocity, residual velocity
Greek letters	
α	impact pitch angle, ballistic yaw angle
δL	projectile erosion
δx_{ijk}	x-component length of ijkth computational cell
$\varepsilon^p, \dot{\varepsilon}^p$	equivalent plastic strain, strain-rate
θ	homologous temperature, obliquity angle

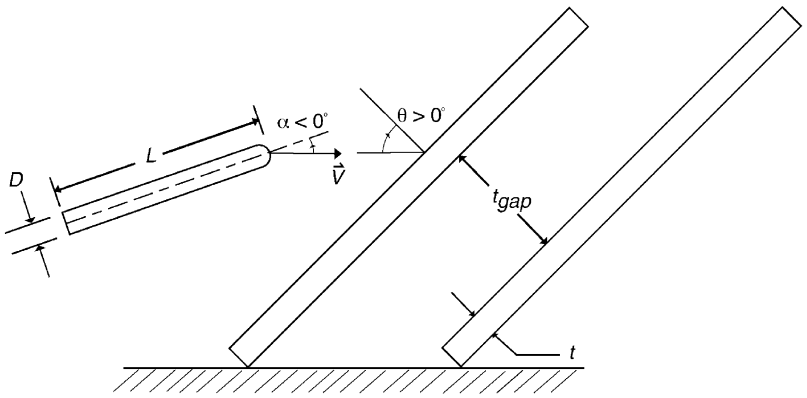

Fig. 1. Schematic of pre-impact geometry (not to scale). Pitch angle is indicated (this is consistent with aerodynamic convention where yaw occurs in the plane orthogonal to the one shown).

tungsten-alloy cylindrical rod projectiles. One- and two-plate spaced target configurations were examined in order to investigate their effect on the perforation and erosion process. The impact geometry is schematically indicated in Fig. 1 and was selected to closely replicate a set of experiments conducted by Bless et al. [2]. In those tests, scatter in the data was due in part to the pre-impact ballistic yaw angle[1] which can arise from launch dynamics, sabot discard effects, and/

[1] Total misalignment angle composed of components in the aerodynamic pitch and yaw planes.

or aerodynamic flow-field effects. In the corresponding simulations only deviations in the aerodynamic pitch angle were investigated, and the impact velocities were exclusively in the hypervelocity regime; $V_0 \in [2.1, 2.6\,\text{km/s}]$.

There have been several studies [3–6] of note in the area of normal and oblique perforation of finite thickness plates. Projectiles included steel and aluminum rods (including spin-stabilized rifle rounds) against a variety of plates including aluminum, mild steel, and carbon steel. Impact velocities were generally under 1 km/s and the intent of the experimental effort was to determine the velocity drop and orientation of the residual projectile. Obliquity angles up to the point where the projectile ricocheted were studied. Forde et al. [5] included L/D 10 tungsten-alloy rods in a reverse impact configuration. This study was novel in that the rods were instrumented with manganin piezo-resistive stress gauges in an attempt to study the stress wave propagation through the rod and to investigate the material response. Additionally, this study for thin plates with t/D 0.5 was augmented with hydrocode analysis. Normandia et al. [6] developed a modified cavity expansion analysis for plate targets. They showed that the target resistance term may depend of the proximity of the rear surface since it may limit the extent of the plastic region.

Holmberg et al. [7] have conducted an experimental investigation with tungsten-alloy rod projectiles and oblique steel plates at impact velocities of 1.5 and 2.5 km/s. Their two-part goals were to determine the applicability of sub-scale experimentation and to investigate the influence of hypervelocity impact. They concluded that sub-scale experimental results were generally applicable and that hypervelocity rods were less affected with respect to post-perforation qualities than were ordnance velocity rods. In a numerical study, Liden et al. [8] found that tungsten projectiles were consumed to a larger extent for higher impact velocities. Gee [9] has investigated the primary erosion and residual erosion (or projectile erosion not directly attributable to plate perforation) for plate targets at hypervelocity. By way of the interface velocity, it was shown how plate gap spacing affected the residual erosion. Penetration and perforation have been described in an empirical manner and for a specific set of experimental conditions by Jeanquartier and Odermatt [10]. There, relationships are presented for the perforation limit and residual length/velocity.

2. Modeling issues

The partial differential equations for penetration mechanics stem from considerations of mass, momentum, and energy balance. A material-dependent constitutive model is also required to complete the formulation and typically includes a dilatational and deviatoric component. An equation of state (EOS) relates the material pressure, density, and internal energy. The Mie–Gruneisen formulation is a popular model for low temperature solids with shock-Hugoniot data as the reference hydrodynamic state. The deviatoric response is governed by a separate part of the constitutive model. Typically, an elastic–plastic strength model is used for J_2-type materials such as metals. The extent of plastic flow is determined by limiting the J_2 invariant using a flow rule, such as von Mises theory, which takes account of the material yield strength. Over-stress is immediately returned to the limit surface via a radial-return type algorithm. Strain and strain-rate dependence are incorporated into the Johnson–Cook [11] model. This model has a simple expression for the flow stress and also includes a term for thermal softening. These modeling

Table 1
Johnson–Cook constitutive model constants

	A (GPa)	B (GPa)	C	n	m	T_M (eV)
Projectile	1.35	0	0.06	1	1	0.1485
Plate	0.7922	0.5095	0.014	0.26	1.03	0.1545

issues are incorporated into the three-dimensional (3D) Eulerian wave-code CTH. McGlaun et al. [12] give an overview of CTH capabilities.

A high resolution square mesh is constructed for the anticipated interaction region and is equivalent to eight computational cells across the rod diameter [13]. Outside of this region, the computational mesh is graded and increases by 4%. Thus, in the graded region (with similar expressions for the y- and z-components),

$$(\delta x_{i+1,j,k} - \delta x_{i,j,k})/\delta x_{i,j,k} = 0.04, \tag{1}$$

where $\delta x_{i,j,k}$ is the x-coordinate length dimension for the i,j,kth cell.

3. Material parameters

Material strength may be affected by strain, strain-rate, and thermal effects. The Johnson–Cook [11] model has proved to be useful in this regard and is given below as

$$Y = [A + B(\varepsilon^p)^n][1 + C\ln(\max\{0.002, \dot{\varepsilon}^p\})][1 - \theta^m], \quad \dot{\varepsilon}^p \leqslant 10^5\ \mathrm{s}^{-1}, \tag{2}$$

where material constants A, B, C, n, m are summarized in Table 1. Strain history dependence is enabled via the equivalent plastic strain, ε^p. The equivalent plastic strain rate, $\dot{\varepsilon}^p$, and homologous temperature, θ, are defined as follows:

$$\dot{\varepsilon}^p = \sqrt{\frac{2}{3}\dot{e}^p_{ij}\dot{e}^p_{ij}}, \quad \theta = \frac{T - T_R}{T_M - T_R}, \tag{3}$$

where $\dot{e}^p_{ij}$ is the plastic strain-rate tensor, T is temperature, and T_R and T_M are the material room and melt temperatures, respectively.

4. Test data

Test data have been drawn from two sources. A complete description of the particular experimental setup may be found in the appropriate reference and only a brief summary is given here for sake of completeness. Bless et al. [2] conducted 15 shots of tungsten-alloy projectiles into oblique, one- and two-plate spaced target configurations. Most of the projectiles were L/D 10 rods with $D = 0.8$ cm (for the cases of interest here). Several velocities were considered as well as several different tungsten alloys. These were primarily W–Ni–Fe or Wi–Ni–Co. The target materials were typically rolled homogeneous armor (RHA) with $t/D \in [0.7, 2.8]$ (although the bulk were t/D 1.6). Pre-impact and post-perforation images were recorded in order to estimate impact

pitch and yaw, residual length, velocity, and orientation.[2] A comment on the pre-impact aerodynamic misalignment angle is in order. Since practically all impacts occur with various amounts of unintended aerodynamic pitch and yaw, the experimental data are sometimes represented with a single number known as the ballistic yaw angle. The magnitude of this angle is usually computed as if pitch and yaw angles are vector components. For small angles, this approximation is more than adequate. The sign of the resultant has been taken from the sign of the pitch component and corresponds to the simulation convention.

The experimental program of Holmberg et al. [7] was conducted with a two-stage light gas gun. Flash radiographs were used to capture the condition of the projectile. However, no ballistic yaw data was included in the report. The L/D 15 projectiles were of a high strength, sintered tungsten-alloy and the plates were armor steel having a Vickers hardness of 300. Two velocities (1.5, 2.5 km/s) were chosen and two target obliquity angles (60°, 80°) were selected. The t/D ratio varied between 0.4 and 1.8 in a manner such that line-of-sight plate thickness was controlled.

5. Numerical results and discussion

As mentioned previously, direct ballistic experimental impact data are usually obtained with various amounts of impact pitch and yaw. This can usually be attributed to aerodynamic effects, sabot discard, or to the natural modes of the projectile. Simulations representing the nominal test conditions [2] have been performed for the impact at 2.6 km/s into one- and two-plate spaced targets including up to $\pm 6^\circ$ of aerodynamic pitch. For all cases here, a residual projectile emerges behind the target. The line-of-sight perforation normalized by the length of eroded projectile (or perforation efficiency) is presented in Fig. 2 for a two-plate target as a function of the ballistic yaw angle. Larger values of the ordinate are favorable since they indicate lesser amounts of erosion, all other things being equal. The results indicate that for $\alpha \in [-6, 0^\circ]$, projectile erosion and line-of-sight perforation are roughly in balance. However, the perforation efficiency is degraded when the impact pitch is positive. As may be seen, the correlation between simulation and test data (open and darkened circular symbols in Fig. 2) is excellent where test data exists. As identified in the computations, the nose-up configuration (with respect to the velocity vector) is slightly favorable for minimizing erosion. This is counter to the results of Anderson et al. [14], who found that the nose-down impact configuration was favorable for similar materials. There, lower perforation times were identified as the significant factor. It should be noted that they used finer aspect ratio projectiles (L/D 20, 36), had slightly more pitch angle deviation, less obliquity, and targets with t/D 1.9.

Additional simulations were performed to evaluate the effect of decreased gap spacing (triangular symbols in Fig. 2). These were for $D = 1$ cm, unless otherwise noted. Clearly, for the smaller gap selected here there is no effective difference in perforation efficiency. It should be mentioned that in [2] if the residual projectile was broken, the reported length was the sum of all segments at least a full diameter D wide. The stated uncertainty in length was $\pm 0.25D$, and since the residual projectile is often broken, the error in residual length may be larger than the stated

[2] Note, flash radiographs were used to determine these properties. The imaging system was not set up, nor was it designed to explore any of the particular erosion mechanisms discussed here.

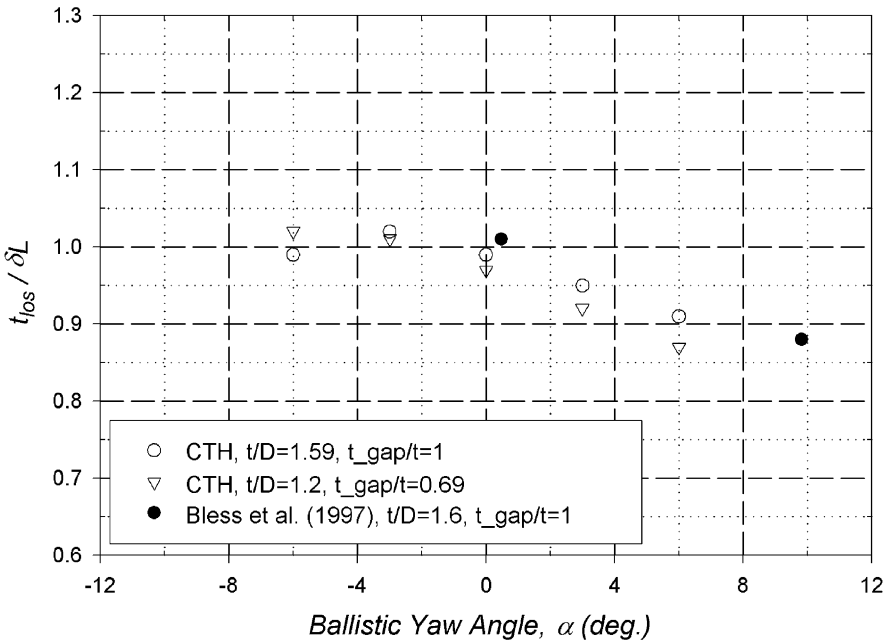

Fig. 2. Line-of-sight perforation normalized by length of eroded projectile; $V_0 = 2.6$ km/s (nom.), L/D 10 tungsten-alloy projectile, two-plate, spaced steel target, $\theta = 65^\circ$.

Table 2
L/D 10 simulation data for oblique impact ($\theta = 65^\circ$)

	2.6 km/s, 1-pl., t/D 1.2, $t_{los} = 2.84$ cm		2.1 km/s, 1-pl., t/D 1.2, $t_{los} = 2.84$ cm		2.6 km/s, 2-pl., t/D 1.2, $t_{los} = 5.68$, $t_{gap}/t = 0.69$		2.6 km/s, 2-pl., t/D 1.59, $t_{los} = 6.01$ cm, $t_{gap}/t = 1$	
α (deg)	δL (cm)	V_R/V_0	δL (cm)	V_R/V_0	δL (cm)	V_R/V_0	δL (cm)	V_R/V_0
0	3.28	0.98	3.0	0.98	5.87	0.96	6.06	0.93
−3	3.12	0.97	2.97	0.96	5.62	0.95	5.91	0.92
−6	3.12	0.96	3.0	0.95	5.55	0.93	6.06	0.90
3	3.37	0.98	3.19	0.97	6.19	0.95	6.34	0.91
6	3.56	0.97	3.28	0.96	6.53	0.93	6.59	0.86

uncertainty. It is worth noting that there is close agreement in residual velocities for the two data sets, Table 2. For the two-plate data analyzed here, $V_R/V_0 \in [0.86, 0.96]$.

Material plots for the extremum cases ($\alpha = -6^\circ, +6^\circ$) illustrate the phenomenology of the penetration and perforation process. For $\alpha = -6^\circ$ (Figs. 3a–e), the material plots show that early time interaction includes the formation of a slot cut into the front face of the first plate, Fig. 3a. This tends to impart a clockwise pitching moment to the projectile and also gives rise to a lateral velocity component. For later times (Figs. 3b and c), the induced rotation tends to re-align the projectile axis along the original velocity vector. Upon exit from the second plate and noting the slight upward change in elevation (Fig. 3d), it can be shown that the late-time path through

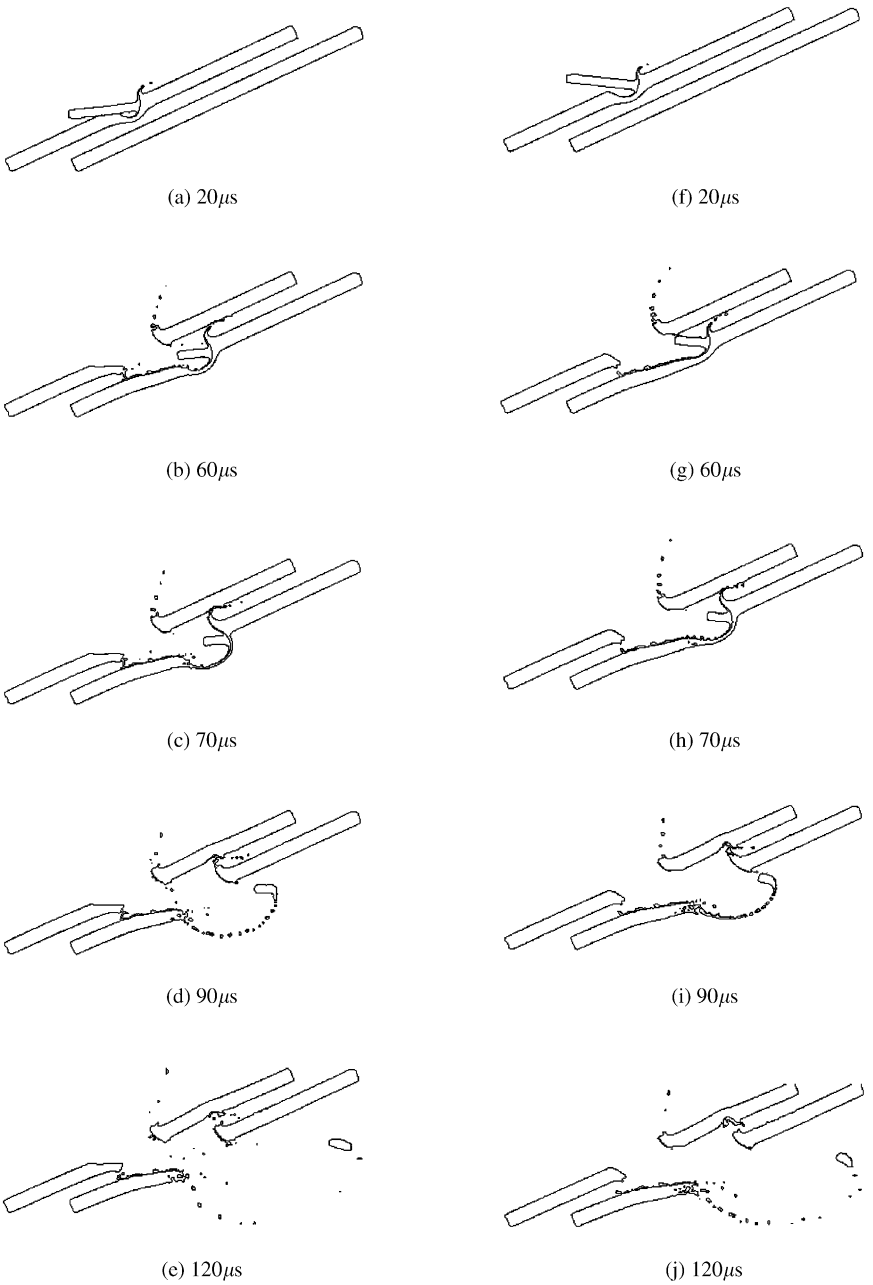

Fig. 3. Material plots for impact of tungsten-alloy projectile into two-plate, spaced steel target at 2.6 km/s: (a–e) $\alpha = -6^\circ$, (f–j) $\alpha = +6^\circ$.

the target is very similar to the $\alpha = 0^\circ$ case. For $\alpha = +6^\circ$ (Figs. 3f–j), the case is noticeably different. Slot formation occurs much later with a slot being cut into the rear face of the front plate, Fig. 3g. The late-time interaction is insufficient to completely re-align the projectile and

upon exit, Fig. 3i, the rod has significant residual rotation. For this case, the pitching moments due to slot interaction and the asymmetric exit conditions are of opposite sense, whereas in the former case the moments are of the same sense. It should be mentioned that the effect of $+6^\circ$ nose-down pitch on perforation efficiency is small and amounts to roughly $0.5D$ of increased erosion. Finally, it appears from the sequence of material plots (specifically, Figs. 3c and 3h) that a small difference in elapsed perforation time exists for the extremum cases. However, the nominal interaction dynamics for the two cases are different due to angle of attack and target obliquity issues and therefore a comparison based solely on equivalent simulation times is not appropriate.

To understand the source for pitch degradation it is instructive to examine the path angles through the targets. For the relatively thin plates considered here, penetration paths through the plates appear similar for the extremum cases. However, it is likely that the nose-down pitch case includes an unfavorable effective path akin to the plates having increased obliquity. That is, the plate appears thicker (Fig. 4). This is similar to the skewed paths obtained from penetration into a semi-infinite thick target when the projectile impacts with pitch angle on the order of the critical angle. Thus the penetration is efficient but the penetration path is not the optimal one. It can be shown that for $\alpha = +3^\circ$, the projectile perforates the target without side-wall interference. For the nose-up pitch case illustrated in Figs. 3a–e, slot interaction immediately re-aligns the projectile and its performance is therefore similar to the $\alpha = 0^\circ$ case.

In addition to angle-of-attack considerations it is also of interest to investigate the effect of impact velocity and of multiple, spaced plates on erosion. Simulations have been performed for L/D 10 projectiles impacting a one-plate target at 2.1 and 2.6 km/s, and one- and two-plate spaced steel targets at 2.6 km/s. These data, along with data from [2,7], are shown in Fig. 5. The test data [2] are for slightly larger t/D and t_{gap}/t ratio. The target obliquity angle, however, corresponds to that numerically simulated. Also, the single-plate data of Holmberg et al. [7] are for different t/D values, L/D values, obliquity angles, and impact velocities. Overall, simulation and test data are reasonably well correlated even though no corrections have been applied to account for mismatch in impact conditions or materials.

The data suggests that the normalized line-of-sight perforation is only mildly sensitive to impact velocity (at least for the velocities considered here) as the differences in erosion amount to approximately $0.25D$ or less for the two impact velocities (open circular and triangular symbols in Fig. 5). However, the trend is inverse in that the lower velocity projectile has slightly higher

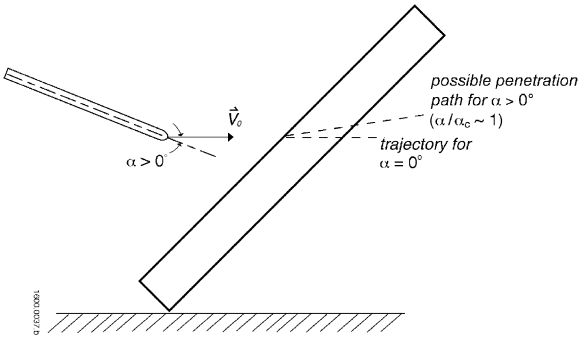

Fig. 4. Schematic of non-optimal penetration path for $\alpha > 0^\circ$.

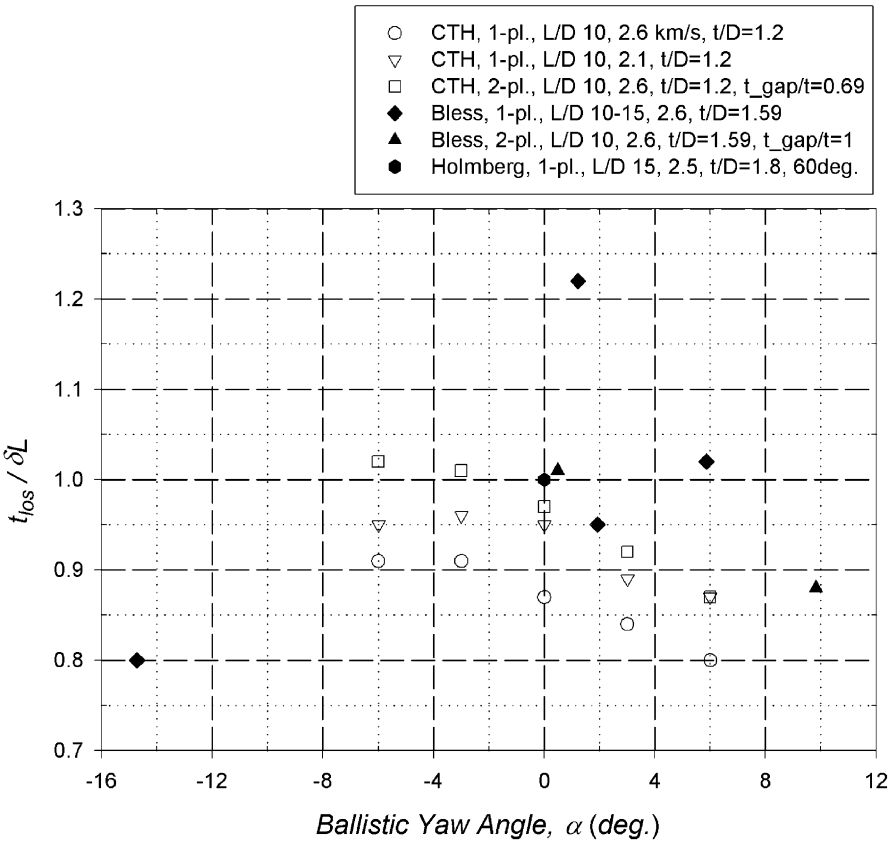

Fig. 5. Line-of-sight perforation normalized by length of eroded projectile. One- and two-plate spaced steel targets with $\theta = 65^\circ$ (unless otherwise noted); L/D 10, 15 tungsten-alloy projectiles.

perforation efficiency. The data also suggests a synergistic effect with respect to erosion in having the second plate close behind the first. This is demonstrated by the higher perforation efficiency (across the ballistic yaw angle range) when comparing the one- and two-plate simulations (open circular and square symbols in Fig. 5). The difference in perforation efficiency for $\alpha = 0^\circ$ corresponds to roughly $0.7D$ less erosion in the two-plate case when compared to the one-plate case. That is, for a simple scaling, the predicted erosion for two single-plate targets spaced far enough apart would be $0.7D$ more than found in the two-plate spaced target modeled here. There are at least two non-mutually exclusive possibilities. One may be that behind-armor-debris from the first plate precedes the projectile into the second plate (Fig. 6a). In this way perforation is initiated by debris rather than projectile. The second effect is related to the gap length between plates. Since a projectile will continue to erode in an air gap due to unequilibrated penetration and tail velocities, maximal erosion will not be attained if the gap length is insufficient to allow for continuing erosion resulting from the residual stress state induced in the projectile as a result of impact with the first plate.

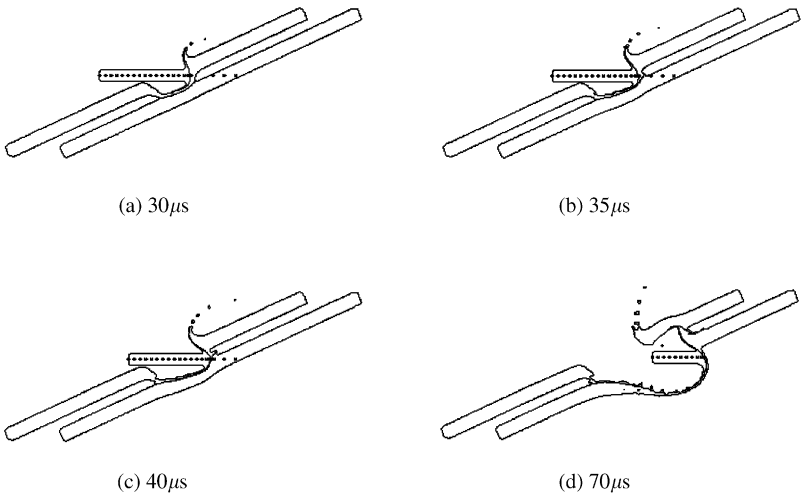

(a) 30μs (b) 35μs

(c) 40μs (d) 70μs

Fig. 6. Material plots for impact of tungsten-alloy projectile into two-plate, spaced steel target at 2.6 km/s and $\alpha = 0^{\circ}$; $t/D = 1.2$, $t_{gap}/t = 0.69$.

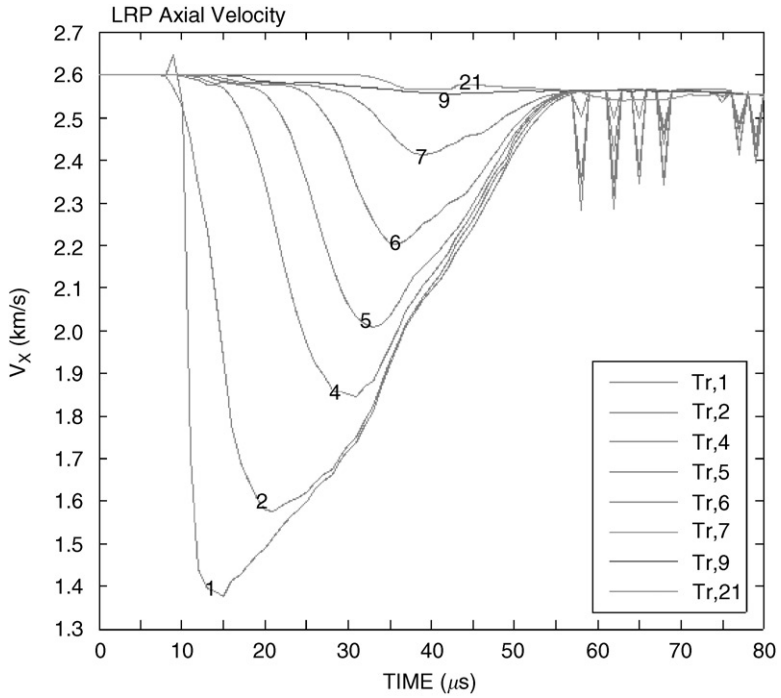

Fig. 7. Axial velocity data for select stations along the projectile while perforating a one-plate steel target at 2.6 km/s and $\alpha = 0^{\circ}$; $t/D = 1.2$.

To explore this idea further we have examined plots of the projectile's axial velocity. The axial velocity component can be used to approximate the interface or penetration velocity if the projectile's lateral velocity component (here, due to oblique impact) is much smaller than the former. This condition is satisfied here. Select axial velocity data for the projectile perforating the one-plate target are displayed in Fig. 7, where Tr.1 denotes "tracer particle 1" and is situated at the tip of the projectile (note, Tr. 21 is situated at the projectile tail). The tracer particles are constrained to remain on shot-line even as the underlying material is eroded. It is not clear from this plot when the projectile breaks out of the plate and therefore when residual (behind-plate) erosion begins. In fact, the calculations for residual erosion to be discussed here are not objective but are thought to be reasonable and conservative. The criterion employed here is to consider residual erosion to have begun when the full projectile diameter has effectively emerged from the rear surface of the plate: that is, when the full diameter clears the exit plane defined by the original rear plate surface.

In Fig. 8, material plots at 35 and 40 μs are seen to bracket the breakout event as defined above. It was estimated that for $t = 38$ μs, the full projectile diameter has emerged from behind the plate. From Fig. 7, the interval for residual behind-plate erosion is $t \in [38, 55\,\mu s]$. At the end of this interval, the penetration and tail velocities are essentially fully equilibrated. Projectile erosion may be computed from the following relation:

$$\dot{L} = (u - v), \tag{4}$$

where u is the penetration or tip velocity and v is the tail velocity. The simple result

$$\delta L = (\tilde{u} - v)\delta t \tag{5}$$

is obtained if $u(t)$ is assumed to vary linearly, and v is taken as constant over the time interval of interest. Hence $\tilde{u}$ in this formulation is the average penetration velocity over the relevant time interval. For $u(t = 38) \cong 2100$ m/s and $v \cong 2550$ m/s, the residual behind-plate erosion may be calculated with the aid of Eq. (5) as $0.38D$.

A similar process is used to calculate residual erosion for the two-plate spaced target. The impact geometry for the first plate of the target array is identical to that just discussed for the one-plate target. Hence, the breakout time from the first plate should correspond to that found for the one-plate target. As may be seen in Figs. 6b and c and in Fig. 9, $t = 38$ μs is approximately the time that the second plate of the two-plate target is initially perforated. This implies that any residual between-plate erosion is unrealized. Using the previous result then, we have considered

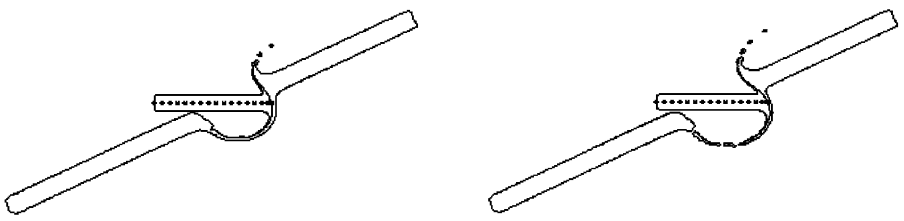

(a) 35μs (b) 40μs

Fig. 8. Material plots for impact of tungsten-alloy projectile into one-plate steel target at 2.6 km/s and $\alpha = 0°$; $t/D = 1.2$.

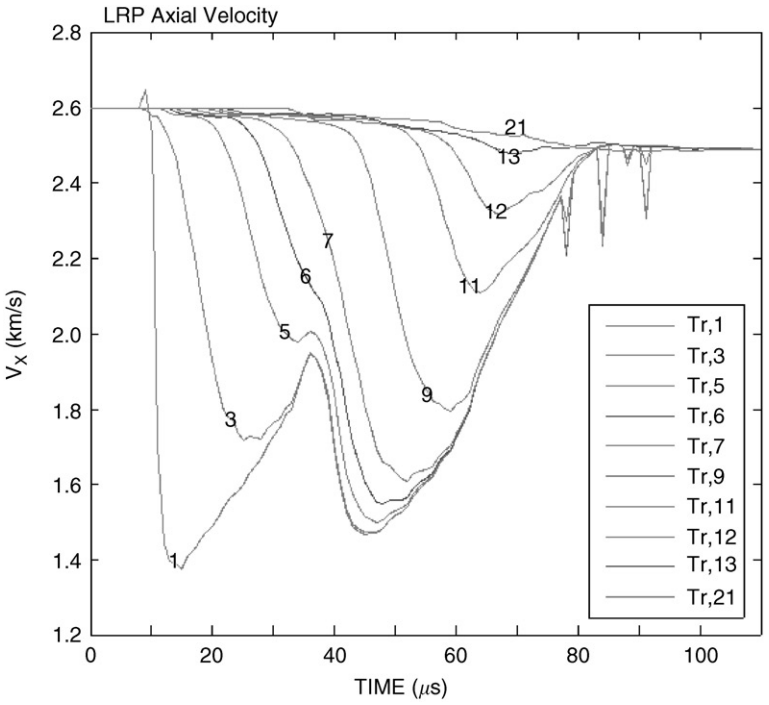

Fig. 9. Axial velocity data for select stations along the projectile while perforating a two-plate, spaced steel target at 2.6 km/s and $\alpha = 0^\circ$; $t/D = 1.2$, $t_{gap}/t = 0.69$.

that $0.38D$ of residual between-plate erosion has gone unrealized due to the proximity of the second plate.

Breakout from the rear plate (plate #2) is qualitatively indicated in Fig. 6d and is estimated to have occurred at $t = 68\,\mu s$. From Fig. 9, the velocity equilibration time is $\sim 82.5\,\mu s$, and this implies that residual behind-plate erosion occurs in the interval $t \in [68, 82.5\,\mu s]$. From Fig. 9, $u(t = 68) \cong 2133\,m/s$ and $v \cong 2493\,m/s$. Assuming linear variation for $u(t) \forall t \in [68, 82.5]$, application of Eq. (5) shows that the behind-plate erosion amounts to $0.26D$. This result and the corresponding result for the one-plate target suggests that residual behind-plate erosion varies with the number of plates in the target array. This is reasonable considering that the tail velocity decreases as a function of the number of plates. Further, as the tail velocity decreases, the time required for velocity equilibration is also seen to decrease, and this directly impacts the erosion calculation. In this way, most of the synergism associated with the two-plate target is seen to arise from unrealized residual between-plate erosion ($0.38D$) which is due to insufficient plate spacing. A second mechanism has been identified from the results which suggests that residual behind-plate erosion decreases as the number of plates in the target array increases ($0.38D$ for a one-plate target vs. $0.26D$ for a two-plate target). This mechanism accounts for $0.12D$ less behind-plate erosion for the two-plate array target (i.e., the difference in the two behind-plate erosion calculations) and implies that it would be inappropriate to simply extrapolate single-plate erosion results and apply

them to multi-plate configurations. It would not be inconsistent, however, to suggest that the two-plate erosion results are—quantitatively—$0.58D$ better, at face value, than for two single plate targets spaced far enough part. However, it has just been shown that the majority of this erosion discrepancy may be attributed to unrealized residual erosion between the plates of the two-plate array target. Finally, we note that the line-of-sight perforation efficiency for the one- and two-plate data [2] show no such synergism as the single-plate data are somewhat scattered. It is difficult to characterize the data [7] since the impact ballistic yaw angle, if non-negligible, was not stated. We have simply plotted it here as if it were for $\alpha = 0^\circ$.

6. Conclusion

Computational experiments were performed for the perforation of thin oblique steel plates by L/D 10 tungsten-alloy projectiles. Primary simulation parameters included impact pitch angle, number of plates, and impact velocity. Additionally, some variation in plate thickness-to-rod diameter ratio and plate gap spacing have been included as well. Normalized line-of-sight perforation efficiency was shown to be only mildly sensitive to impact velocity (at least for the velocities considered here). Furthermore, it was shown that erosion through a two-plate, spaced target was not simply a scalar multiple of the single-plate case. The data suggest that residual behind-plate erosion varies with the number of target plates, decreasing as the number of plates increases. This was due to deceleration of the tail and, also, the corresponding decrease in the time interval for which the penetration and tail velocities are unequilibrated. For a second plate close behind the first, some synergism, with respect to erosion, was evident. However, it was demonstrated that this was due in large part to unrealized residual between-plate erosion as a result of insufficient plate spacing. It was also shown that perforation efficiency was sensitive to small amounts of impact pitch. For late-times, the nose-up case ($\alpha < 0^\circ$) appears indistinguishable from the $\alpha = 0^\circ$ case due to early slot formation and asymmetric exit conditions, and in these cases the perforation efficiencies are similar. The nose-down cases ($\alpha > 0^\circ$) have degraded perforation efficiencies that are likely due to physically longer paths through the target. Finally, it was seen that the numerical data generally compared favorably with archival test data conducted under similar conditions.

Acknowledgements

The research reported in this paper was performed in connection with Contract number DAAD17-01-D-0001 with the US. Army Research Laboratory (ARL). The views and conclusions contained in this paper are those of the author and should not be interpreted as presenting the official policies or position, either expressed or implied, of the US. Army Research Laboratory or the US. Government unless so designated by other authorized documents. The US. Government is authorized to reproduce and distribute reprints for Government purposes notwithstanding any copyright notation hereon. The author gratefully acknowledges Dr. David Littlefield and Dr. Sikhanda Satapathy for valuable discussions on this work.

References

[1] Gee DJ, Littlefield DL. Yaw impact of rod projectiles. Int J Impact Eng 2001;26:211–20.
[2] Bless SJ, Pedersen B, Campos J, Normandia MJ, Subramanian R. Penetration of oblique plates. IAT.R 0149, Institute for Advanced Technology, The University of Texas at Austin, Austin, TX, 1997.
[3] Goldsmith W, Finnegan SA. Normal and oblique impact of cylindro-conical and cylindrical projectiles on metallic plates. Int J Impact Eng 1986;4(2):83–105.
[4] Gupta NK, Madhu V. Normal and oblique impact of a kinetic energy projectile on mild steel plates. Int J Impact Eng 1992;12(3):333–43.
[5] Forde LC, Bourne NK, Rosenberg Z, Cornish R, Lynch NJ, Cullis IG, Church PD. Experimental investigation and analysis of penetration in oblique impact. Proceedings of the 16th International Symposium on Ballistics, San Francisco, CA, 1996. p. 641–9.
[6] Normandia MJ, Satapathy S, Littlefield DL, Anderson CE. Modified cavity expansion analysis for modeling finite target penetration. Proceedings of the 16th International Symposium on Ballistics, San Francisco, CA, 1996. p. 219–28.
[7] Holmberg L, Lundberg P, Westerling L. An experimental investigation of WHA long rods penetrating oblique steel plates. Proceedings of the 14th International Symposium on Ballistics, Quebec, Canada, 1993. p. 515–24.
[8] Liden E, Ottosson J, Holmberg L. WHA long rods penetrating stationary and moving oblique steel plates. Proceedings of the 16th International Symposium on Ballistics, San Francisco, CA, 1996. p. 703–11.
[9] Gee DJ. Oblique plate perforation by slender rod projectiles. Proceedings of the 19th International Symposium on Ballistics, Interlaken, Switzerland, 2001. p. 1123–32.
[10] Jeanquartier R, Odermatt W. Post-perforation length and velocity of KE projectiles with single oblique targets. Proceedings of the 15th International Symposium on Ballistics, Jerusalem, Israel, 1995. p. 245–52.
[11] Johnson GR, Cook WH. A constitutive model and data for metals subjected to large strains, high strain rates and high temperatures. Proceedings of the 7th International Symposium on Ballistics, The Hague, Netherlands, 1983. p. 541–7.
[12] McGlaun JM, Thompson SL, Elrick MG. CTH: A three-dimensional shock wave physics code. Int J Impact Eng 1990;10:351–60.
[13] Littlefield DL, Anderson CE. A study of zoning requirements for 2-D and 3-D long-rod penetration. Proceedings of the APS Topical Group on Shock Compression of Condensed Matter, Seattle, WA, 1995. p. 1131–4.
[14] Anderson CE, Bless SJ, Sharron TR, Satapathy S, Normandia MJ. Investigation of yawed impact into a finite target. Proceedings of the APS Topical Group on Shock Compression of Condensed Matter, Amherst, MA, 1997. 925p.